Monthly Notices
of the
ROYAL ASTRONOMICAL SOCIETY

MNRAS **497,** 5507–5517 (2020)
Advance Access publication 2020 June 2

doi:10.1093/mnras/staa1508

Intensity and time series of extreme solar-terrestrial storm in 1946 March

Hisashi Hayakawa [1,2,3,4★] Yusuke Ebihara,[5,6] Alexei A. Pevtsov [7,8★] Ankush Bhaskar,[9,10] Nina Karachik[11] and Denny M. Oliveira[9,12]

[1]*Institute for Space-Earth Environmental Research, Nagoya University, Nagoya 4648601, Japan*
[2]*Institute for Advanced Researches, Nagoya University, Nagoya 4648601, Japan*
[3]*UK Solar System Data Centre, Space Physics and Operations Division, RAL Space, Science and Technology Facilities Council, Rutherford Appleton Laboratory, Harwell Oxford, Didcot, Oxfordshire OX11 0QX, UK*
[4]*Nishina Centre, Riken, Wako 3510198, Japan*
[5]*Research Institute for Sustainable Humanosphere, Kyoto University, Uji 6110011, Japan*
[6]*Unit of Synergetic Studies for Space, Kyoto University, Kyoto 6068306, Japan*
[7]*National Solar Observatory, 3665 Discovery Drive, 3rd Floor, Boulder, CO 80303, USA*
[8]*Central Astronomical observatory of Russian Academy of Sciences at Pulkovo, Saint Petersburg 196140, Russia*
[9]*NASA Goddard Space Flight Center, Greenbelt, MD 20771, USA*
[10]*Catholic University of America, Washington, DC 20017, USA*
[11]*Ulugh Beg Astronomical Institute of the Uzbekistan Academy of Sciences, Tashkent 100052, Uzbekistan*
[12]*Goddard Planetary Heliophysics Institute, University of Maryland, Baltimore County, Baltimore, MD 201740, USA*

Accepted 2020 May 20. Received 2020 May 14; in original form 2020 April 17

ABSTRACT

Major solar eruptions occasionally cause magnetic superstorms on the Earth. Despite their serious consequences, the low frequency of their occurrence provides us with only limited cases through modern instrumental observations, and the intensities of historical storms before the coverage of the Dst index have been only sporadically estimated. Herein, we examine a solar-terrestrial storm that occurred in 1946 March and quantitatively evaluate its parameters. During the ascending phase of Solar Cycle 18, two moderate sunspot groups caused a major flare. The Hα flaring area was recorded to be $\geq$600–1200 millionths of solar hemisphere, suggesting that this was an M- or X-class flare in soft X-ray intensity. Upon this eruption, a rapid interplanetary coronal mass ejection (ICME) with an average speed of $\approx$1590 km s^{-1} was launched. Based on measurements in four known mid-latitude and relatively complete magnetograms, the arrival of this extreme ICME caused a magnetic superstorm, which caused an initial phase with the H-component amplitude of $\geq$80 nT, followed by a main phase whose intensity was reconstructed as ≤ -512 nT using most negative Dst$*$ estimates. Meanwhile, the equatorial boundary of the auroral oval extended down to $\leq$41°.8 in invariant latitude and formed a corona aurora in Watheroo, Australia. Interestingly, during this magnetic superstorm, larger magnetic disturbances were recorded at dusk and near the dip equator on the dayside. Its cause may be associated with a strong westward equatorial electrojet and field-aligned current, in addition to the contribution from the storm-time ring current.

Key words: Sun: coronal mass ejections (CMEs) – Sun: flares – sunspots – planets and satellites: aurorae – planets and satellites: magnetic fields.

1 INTRODUCTION

Solar eruptions such as flares and coronal mass ejections (CMEs) may direct interplanetary CMEs (ICMEs) toward the Earth and trigger geomagnetic storms. The strongest storms are usually associated with the southward interplanetary magnetic field (IMF) in the leading edge of the ICMEs (Gonzalez et al. 1994; Daglis et al. 1999; Lockwood et al. 2016). Investigations into such storms, particularly extreme ones, are important for an assessment of the effects on the near-Earth space and ground environments (Cliver & Dietrich 2013; Miyake, Usoskin & Poulianov 2019), as well as on the technological infrastructure that modern societies rely heavily upon (Baker et al. 2008; Riley et al. 2018). Statistical studies of such extreme events may provide important clues regarding the likelihood of their occurrence and their potential economic impact (Oughton et al. 2017; Riley et al. 2018; Chapman, Horne & Watkins 2020).

The disturbance storm time (Dst) index is commonly used to assess the strength of geomagnetic disturbances. The Dst is computed as the average horizontal component of the Earth's magnetic field measured hourly at four geomagnetic observatories situated in the mid-latitude regions (Sugiura 1964; World Data Center for Geomagnetism, Kyoto et al. 2015). Since the introduction of the Dst in 1957, the most extreme geomagnetic storm (or superstorm) occurred in 1989 March (most negative Dst $= -589$ nT). This magnetic superstorm caused major electric power blackouts and multiple power disruptions in Canada and the United States, as well as worldwide radio communication failures (Allen et al. 1989; Boteler 2019). A recent analysis suggests the possibility of even stronger societal consequences of geomagnetic superstorms, when projecting superstorms that occurred in 1859 September and 1921 May into a contemporary context (Baker et al. 2008; Riley et al.

* E-mail: hisashi@nagoya-u.jp (HH); apevtsov@nso.edu (AAP)

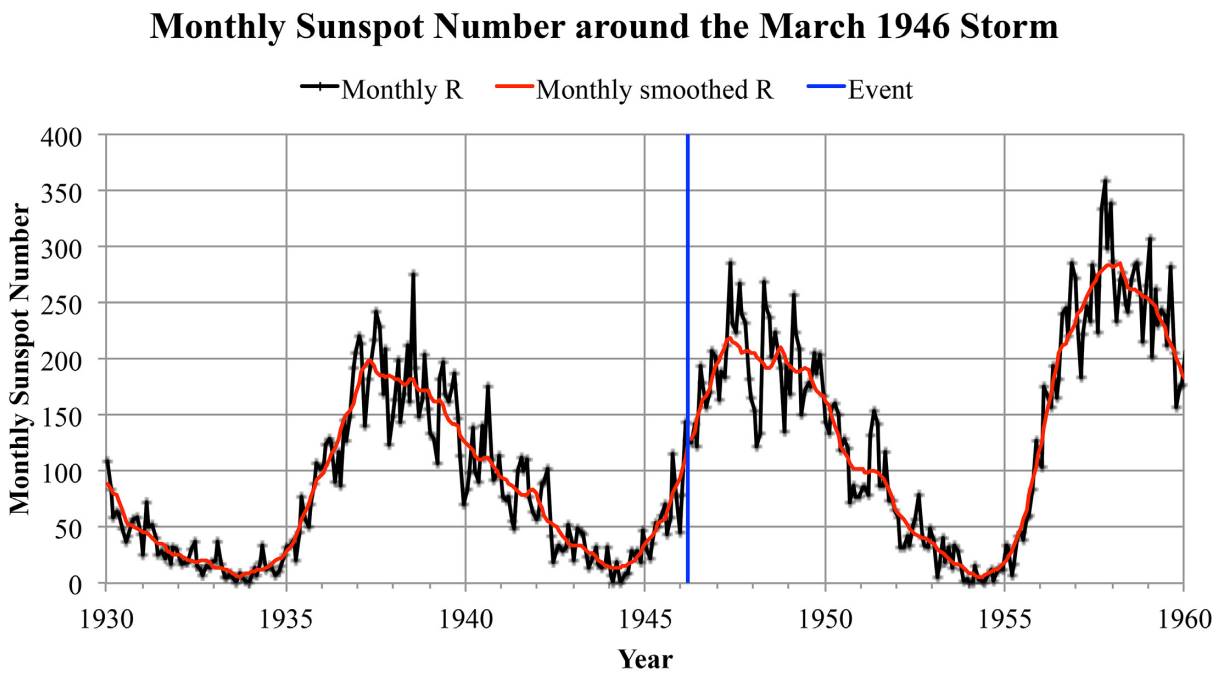

Figure 1. Monthly number of sunspots (R) located near the 1946 March storm event (1930–1960) derived from WDC SILSO (Clette & Lefevre 2016), where the monthly R, monthly smoothed R, and occurrence time of the storm are shown as black, red, and blue vertical lines, respectively.

2018). Large-intensity geomagnetic superstorms (Dst ≤ -500 nT) are rare (Riley et al. 2018). Thus, as an example, the second largest geomagnetic storm within the coverage of the standard Dst index occurred in 1957 July (Dst $= -429$ nT), and we have a relatively large gap in intensity between the largest and second largest storms, as measured by Dst index (World Data Center for Geomagnetism, Kyoto et al. 2015). This motivated us to extend our measurements back in time, although doing so is challenging owing to the fragmental and scarce availability of contemporary magnetic measurements. For example, the intensities of the 1859 September and 1872 February storms remain controversial because only the Colaba magnetogram is currently available for these storms in mid- to low magnetic latitudes without going off-scale (Tsurutani et al. 2003; Cliver and Dietrich 2013; Hayakawa et al. 2018; Lakhina & Tsurutani 2018). Nevertheless, three superstorms have been measured using procedures equivalent to those applied in most negative Dst estimates (which we refer to as Dst$*$), with caveats of occasional usage of equivalent stations: the superstorms in 1903 November (Dst$* \approx -531$ nT), 1909 September (Dst$* \approx -595$ nT), and 1921 May (Dst$* \approx -907 \pm 132$ nT) (Hayakawa et al. 2019a,b, 2020; Love, Hayakawa & Cliver 2019a, b).

In this context, we extend our investigations to the 1946 March storm. This storm is ranked as the seventh largest using the classic *aa* index, which has been available since 1868 (Lefèvre et al. 2016), and the second largest using the deviation of the horizontal force (H) at Greenwich Observatory available between 1874 and 1955 (Jones 1955). This storm was so intense that the Kakioka magnetogram went off-scale according to the Kakioka Event Database.[1] Although these facts highlight the intensity of the 1946 March storm, its occurrence immediately after World War II, resulting in incomplete measurements, has made it difficult to determine its actual intensity. Therefore, in this study, we investigate this superstorm based on its source active region, its solar eruption, its storm intensity and time series, and its consequences.

2 SUNSPOT AND SOLAR ERUPTION

In 1946 March, the Sun was in the ascending phase of Solar Cycle 18 (smooth monthly sunspot number $R = 80.0$). Starting from the transition of the minimum of Solar Cycles 17 and 18 in 1944 February ($R = 0.8$), the sunspots increased to the maximum number in 1947 May ($R = 285.0$, Fig. 1). On 1946 March 27, two moderate-sized sunspot groups were situated in the Northern hemisphere close to the central meridian. One of these groups, with an area of 492 millionths of solar hemisphere (msh) situated at a latitude of N19°–20° and an E5° central meridian distance, was associated with a large solar flare (D'Azambuja 1947, p. 32; Jones 1955, pp. 79–82). As summarized by D'Azambuja (1947, p. 32), this flare was observed at Kodaikanal and Tachkent (i.e. Tashkent) during 4:10–4:45 GMT (max. intensity at 4:18) and during 4:30–7:32 GMT (with a note regarding 'two eruptive centers'), respectively. Its intensity in terms of Hα flare classification was recorded as 3 at both observatories, indicating a flare area of 600–1200 msh (Švestka 1976, p. 14).

Original observational logbooks at Tashkent (*Journal of Spectrohelioscopic Observations* № 42, observation № 29, pp. 98–100; *Catalogue of Solar Rapid Processes* № 4, observation № 15, p. 11) reveal further details of this flare beyond the brief description by D'Azambuja (1947, p. 32). At that time, routine observations at the Tashkent Astronomical Observatory (currently Ulugh Beg Astronomical Institute of the Uzbekistan Academy of Sciences) were conducted using a spectrohelioscope built by Howell and Sherburne (Pasadena, California). A detailed description of this instrument can be found elsewhere (Hale 1929). In 1941, the instrument was modified to enable photographic observations.

[1] http://www.kakioka-jma.go.jp/obsdata/Geomagnetic_Events/Events_index.php.

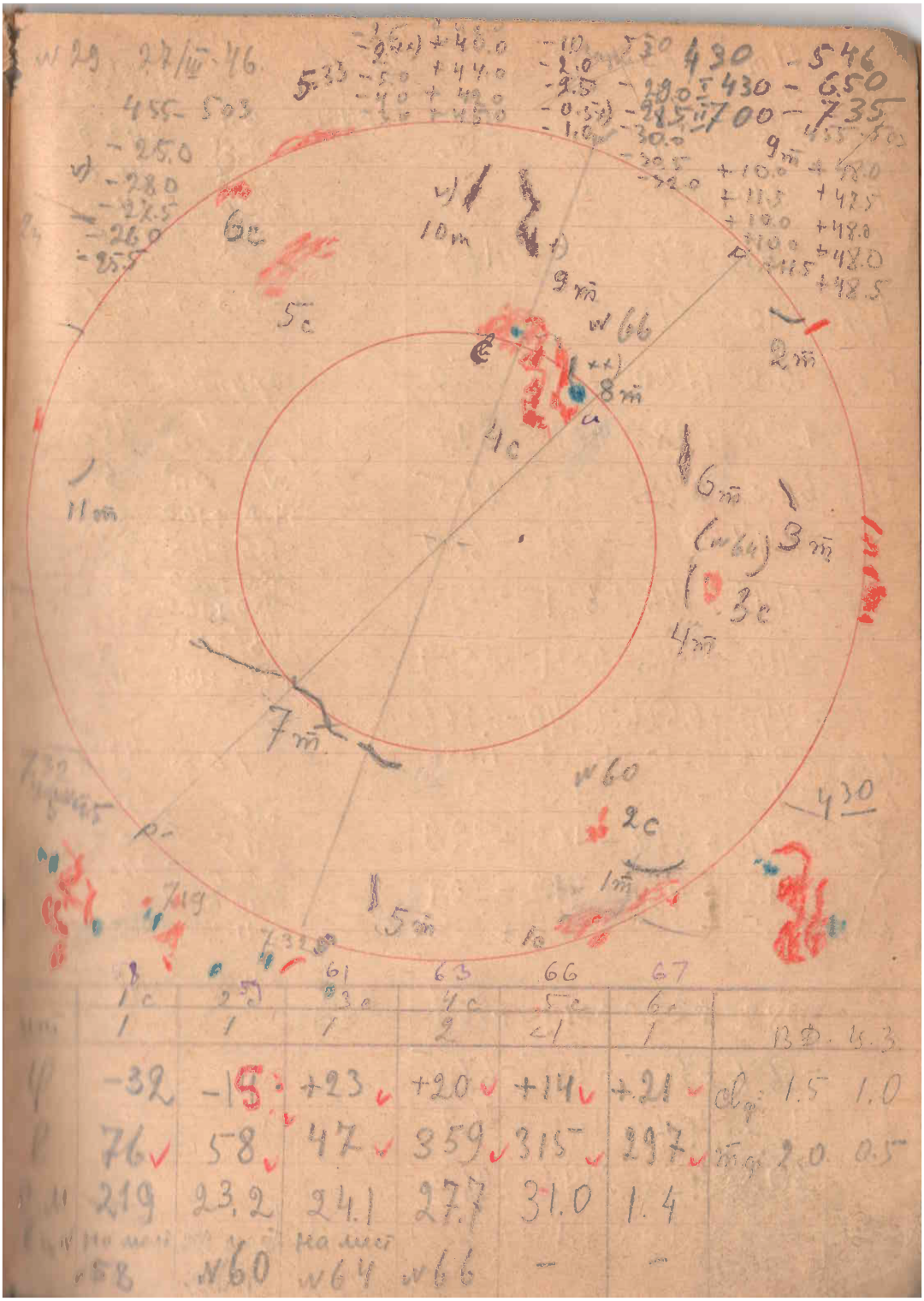

Figure 2. Daily drawing of solar activity in Hα observed on 1946 March 27 (*Journal of the Spectroheliosc opic Observations* № 42, observation № 29, p. 98). The solar disc is outlined by the red circle with the larger radius, with courtesy of Ulugh Beg Astronomical Institute (UBAI) of the Uzbekistan Academy of Sciences. A circle with a smaller radius marks the central part of the solar disc. Two lines crossing the disc mark the direction of the geocentric north pole (PP') and the solar rotational north pole. Dark floccule (the chromospheric filaments) are drawn using a regular pencil, and bright floccule (plage) and prominences are shown by the red pencil marks. Sunspot locations are identified by the blue pencil marks.

Fig. 2 shows a drawing from the observer's logbook for 1946 March 27.

In addition to recording the locations and appearances of different solar features, the observer also made additional sketches to follow the changes of the most important features. These sketches are shown below the full-disc drawing. On the right-hand side of the image, the drawing shows the appearance of the flaring region at 4:30 GMT (beginning of the observations). The next sketch was taken

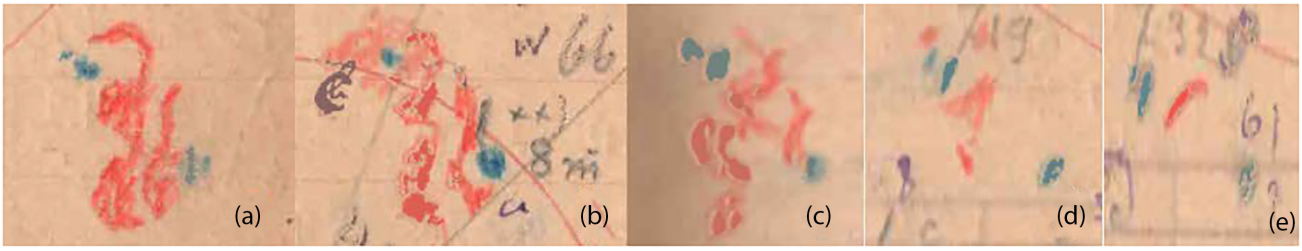

Figure 3. Excerpts from a daily drawing of solar activity in Hα observed on 1946 March 27 at Tashkent Astronomical Observatory at (panel a) 4:30 GMT, (panel b) 4:55–5:03 GMT (time of the main/summary drawing of the full disc), (panel c) 5:45 GMT, (panel d) 7:19 GMT, and (panel e) 7:32 GMT, with courtesy of Ulugh Beg Astronomical Institute (UBAI) of the Uzbekistan Academy of Sciences. The sunspot locations are identified by the blue pencil marks. Flare ribbons (and bright plages) are shown by the red pencil. A small filament, which later erupted and disappeared, is shown in panel (b) with a regular pencil mark with two cross marks next to it. Sketches were scaled to each other and rotated to approximately match the location of the two large spots. The red arc in panel (b) corresponds to a portion of a circle marking a 30° distance from the solar disc centre. The two straight lines in panel (b) show the orientation of the image with respect to the geocentric north pole (lower line) and the solar rotational north pole (upper line).

at 5:45 GMT (shown on the left-hand side of the image). Two more sketches shown to the right from the latter sketch were taken at 7:19 and 7:32 GMT (end of the observations). The orientation of the sketches (based on the line connecting two sunspots (blue dots) changes between the sketches taken during 4:30–5:45 and 7:19–7:32 GMT. The spectrohelioscope was fed using two coelostat mirrors, and this change in orientation could be related to the change in the position of the second coelostat mirror from the west to east. Fig. 3 shows the excerpted time series of the solar flare from the full-disc drawing in Fig. 2. Visually, the appearance of bright areas in this region is reminiscent of a two-ribbon flare. This is consistent with the strong flare of importance 3 reported by the Tashkent observatory. However, note that the Bulletin observatory (1943) used a slightly different system in its early observations to characterize flares and their importance. To characterize weak flares, a 1b class was added to the classification used by the *Quarterly Bulletin on Solar Activity.*

The observatory's catalogue of flares provides the following report (translated from Russian from the Catalogue of Solar Rapid Processes № 4, observation № 15, p. 11): 'An eruption in group No. 66 with two strong erupting centres. At 4:30 (beginning of observations), the eruption was at its maximum. By 5:45, two large centres began disintegrating into smaller kernels. The brightness slowly decreased. At 5:30, a dark-erupting floccule was identified with an eruption speed of 77 km s^{-1}. The southern end of this floccule was located in the sunspot umbrae. By 6:34, this dark floccule had disappeared. By 7:32, the eruption process ended'.

From this, we have improved our understanding of the brief descriptions for D'Azambuja (1947, p. 32). The onset of the Tashkent flare observation occurred at 04:30 GMT and the flare had already been 'at its maximum'. This explains the apparent discrepancy with the flare duration of '4:10–4:45 GMT (max. intensity at 4:18)' reported at Kodaikanal. It seems that Tashkent observers missed the maximum of this flare (4:18 GMT) and started their observations slightly after its occurrence (4:30 GMT). They then recorded the sequence of this flare from 4:30 GMT until its end at 7:32 GMT.

The Hα drawing and enlarged sketches depict this flare with two ribbons with 'two eruptive centers' (D'Azambuja 1947, p. 32) and indicate relatively large flare ribbons between two active regions (Toriumi et al. 2017). Indeed, large quiescent filaments were confirmed in Hα images at the Meudon spectroheliograph at that time (Fig. 4). From these images, it is concluded that a large quiescent filament north of the eruption site did not erupt. Instead, some active region filament(s), located between two active regions, may have erupted on March 27 and then reformed on the same day. These filaments did not seem to change much on March 28.

Using this drawing, we estimated the flare area to be approximately 2600–2900 msh at 4:30 GMT, which corresponds to a flare importance of '3+'. Because this was after the brightness maximum at 4:18 GMT, we conservatively confirm that the flare importance was at least comparable to the optical flare measurements of '3' reported by D'Azambuja (1947, p. 32). A dark-erupting floccule, which can be identified in a full-disc drawing, showed a speed of approximately 77 km s^{-1}, which seems to be in agreement with typical velocities of filament in the early phases of their eruption (see fig. 2 in Balasubramaniam et al. 2011). Using sketches made for 4:30 and 5:45 GMT, we estimated the flare–ribbon separation speed as 8 km s^{-1}, which is in general agreement with a recent study of two-ribbon (eruptive) flares (see Hinterreiter et al. 2018).

Strong optical flares of importance 3 are usually related to strong X-class flares in a soft X-ray fluence, whereas the opposite is not true because X-class flares may have extremely weak subflare optical counterparts. To demonstrate this, we used flare reports compiled by NOAA's National Center for Environmental Information (NCEI) at Boulder, Colorado.[3] Only data from 1982–2008 reports were used because flare reports before 1982 and after 2008 do not provide information regarding X-ray flares. We selected all flare entries, which list both the importance of optical (Hα) flares and their X-ray class for the same event. Out of 26 380 events, there were only 97 flares with an optical importance of 3. In 64 (66 per cent) of the cases, optical flares with an importance of 3 were associated with X-class flares. In 29 (30 per cent) of the cases, there were M-class flares. In the remaining four (4 per cent) cases, Hα flares with an importance of 3 were associated with C-class flares in soft X-ray fluence. Based on these statistics, it is probable that the flare event on 1946 March 27 was associated with a major X-class or at least an M-class X-ray flare.

3 INTERPLANETARY CORONAL MASS EJECTION

A study of CMEs observed with the Large Angle and Spectrometric Coronagraph (LASCO; Brueckner et al. 1995) aboard the Solar and Heliospheric Observatory (SOHO; Domingo, Fleck & Poland 1995) during 1996–2010 showed that 90 per cent of X-class flares

[2]http://bass2000.obspm.fr/piwigo/index.php?/category/619/start-30.

[3]https://www.ngdc.noaa.gov/stp/solar/solarflares.html.

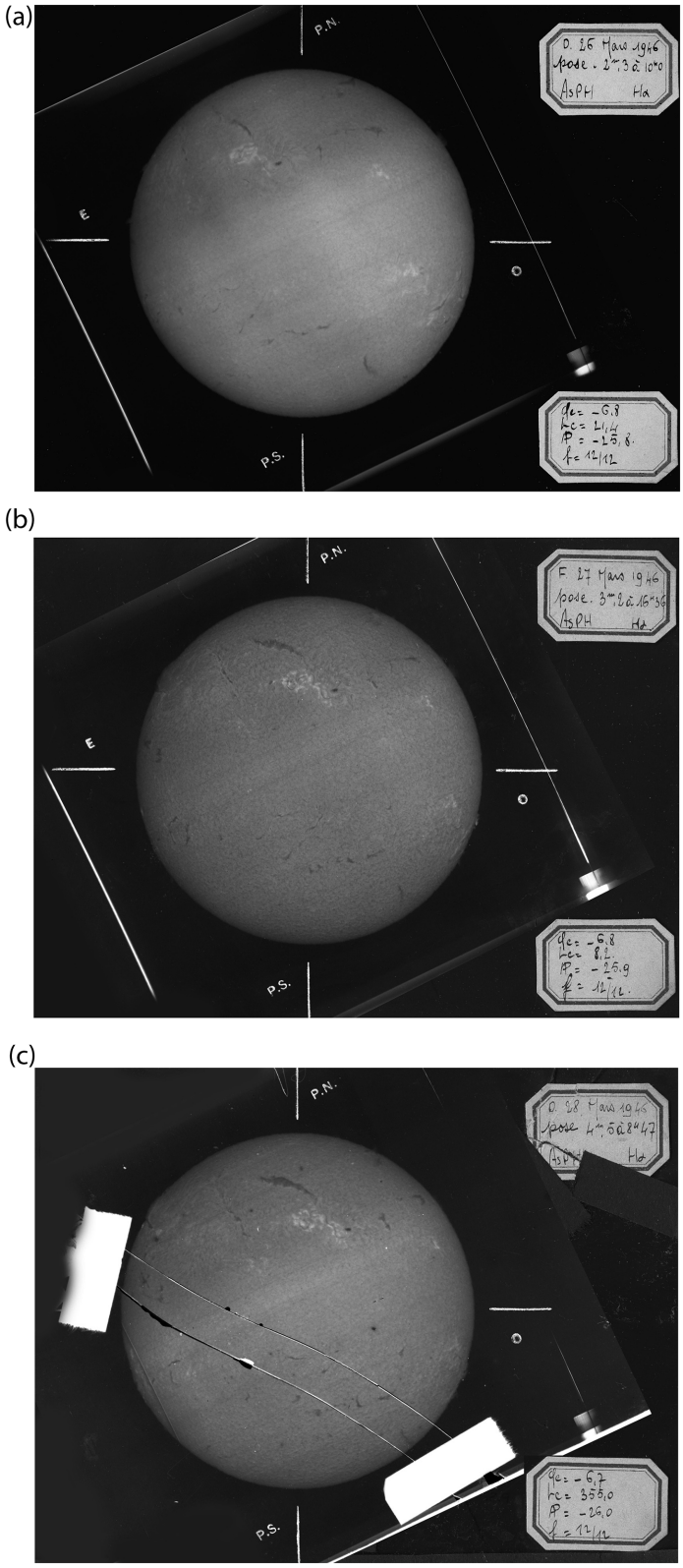

Figure 4. Meudon spectroheliograph on 1946 March 26 (upper panel), 27 (middle panel), and 28 (lower panel) derived from the BASS200 Database of the Solar Survey Archive, with courtesy of the Paris Observatory.[2] A large quiescent filament located north to a large bright plage and east to a large sunspot (upper part of solar disc image) is present in all three days, and thus does not appear to erupt as part of this event. A small active region filament can be seen to the east (left-hand side) of the sunspot between two narrow strips of bright plages. This filament is also present in all three days of observations, but it appears longer on March 26 (upper panel), as compared with the next two days (middle and lower panels). The latter may suggest that a portion of this active region filament had erupted on 1946 March 27 and perhaps reformed after the eruption.

are associated with a CME. For M-class flares, the association was lower at 30 per cent (Youssef 2012). Based on these statistics, it is plausible that an ICME was launched during the major flare on 1946 March 27. It arrived at Earth at 6:35–6:36 GMT on March 28 as evidenced by the commencement of a globally reported significant storm sudden commencement (SSC; Table 1). Assuming a flare onset at ≈4:30 GMT, the recorded SSC at 6:35–6:36 GMT indicates the transit time of this ICME as ≈26.1 h, whereas the absence of coronagraph and *in situ* satellite observations in the solar wind does not allow us to accurately establish the exact timing of ICME eruption and accommodate uncertainty for this transit time. The combined uncertainties are probably within several tens of minutes, given the uncertainty in the time of the flare maximum, and the time when the CME eruption started relative to the flare peak. As an indication of these uncertainties, the values of our estimates are used with the '≈' sign.

Accordingly, we estimated the average Earthward propagation speed of this ICME as ≈1590 km s^{-1}. The SSC amplitudes have mostly been reported to be ≥80 nT, whereas they are more significant at the nightside (Tucson and Huancayo). The greater amplitude of the SSC at the nightside is empirically known (Ferraro & Unthank 1951) and associated with field-aligned currents (Shinbori et al., 2009, 2012). Further, by following Siscoe, Formisano & Lazarus (1968) and Araki (2014), we carried out first-order estimates of the solar wind dynamic pressure jump and the downstream solar wind density. By assuming a background/upstream solar wind pressure of 2 nPa to observe an ≈80-nT change in the low-latitude geomagnetic field at the ground, we need to have a downstream solar wind pressure of ≈45.5 nPa and a density of ∼12 cm^{-3} if the shock is traveling at a speed of ≈1590 km s^{-1}. Note that these estimates are approximate and can vary because of the lack of *in situ* measurements of solar wind and IMF during this period, and we do not have an exact idea of the associated characteristic of the contemporary solar wind conditions. The CME speed is estimated using the Sun–Earth distance on the day of observations and the time between the flare eruption and the onset of the geomagnetic storm. This is an average speed, which does not take into account a gradual acceleration of the CME at the beginning of its eruption and subsequent possible deceleration due to the solar wind drag during the propagation (see e.g., Gopalswamy 2018).

4 TIME SERIES AND INTENSITY OF THE 1946 MARCH STORM

The arrival of this powerful ICME resulted in a significant magnetic storm. Indeed, this storm was considered the second largest at Greenwich (1660 nT) during 1874–1954 and the seventh largest in the classic *aa* index (Jones 1955, p. 79; Lefevre et al. 2016). Therefore, it is of significant interest to compare its intensity with modern storms in the space age scaled with the standard Dst. This index is derived from the horizontal component of the geomagnetic field at four mid-latitude stations. The large negative values of the Dst are used to estimate the strength of the ring current. The standard stations (see Table 1) were set as Honolulu (Hawaii), San Juan (Puerto Rico), Hermanus (South Africa), and Kakioka (Japan), and the data series were computed in the WDC for Geomagnetism at Kyoto (Sugiura 1964; World Data Center for Geomagnetism, Kyoto et al. 2015). This major geomagnetic storm was also recorder by mid-latitude stations across USSR (Afanasyeva 1954), but these data were not used in calculation of the Dst, and thus are not discussed here.

However, it is a challenge to extend this index to the 1946 March storm because this storm was too intense for contemporary magnetograms and hence was recorded quite incompletely. Even in the standard Dst stations, Kakioka was off-scale during 12:00–15:00 GMT and only incompletely recorded its H amplitude as >412 nT (see Table 1). This affects any estimates with standard stations (e.g., Karinen & Mursula 2005). Therefore, we need to replace Kakioka with another mid-latitude station situated at a similar magnetic longitude. The location of Watheroo, Australia, is favourable in this sense and fills the geographical gap of the other three standard Dst stations. Here, the magnetogram, off-scale only during 14:06–14:23 GMT (see Parkinson 1946), and the hourly value were registered in the existing data set. Their profiles are summarized in Table 1 along with their geographic and geomagnetic coordinates.

Deriving these data from the WDC for Geomagnetism at Kyoto,[4] we followed the calculation procedure of the Dst index. Sugiura (1964) and World Data Center for Geomagnetism, Kyoto et al. (2015) defined the magnetic disturbance at the given stations (D_i (t)), removing the baseline (B_i) and the solar quiet (Sq) daily variations (Sq_i (t)) from the recorded horizontal force (H_i (t)). This is described through equation (1):

$$D_i(t) = H_i(t) - B_i - Sq_i(t), \tag{1}$$

$$\mathrm{Dst}(t) = \frac{1}{4}\sum_{i=4}^{4}\frac{D_i(t)}{\cos(\lambda_i)}. \tag{2}$$

Here, we approximate B_i with the annual mean of each reference station derived from the WDC for Geomagnetism at Edinburgh[5]. We also approximated Sq_i (t) with the average daily variations in these stations for the five quietest days in 1946 March (3, 8, 12, 16, and 19) on the basis of the corrected *aa* index by Lockwood et al. (2018). For each quiet day and station, we conducted a mid-night subtraction separately. This helped us eliminate any magnetospheric contributions during each quiet day. To compute the Dst estimate, the magnetic disturbance in each reference station (D_i (t)) is weighted with their magnetic latitude (λ; see Table 1) and then averaged for each hour, as shown in equation (2).

Fig. 5 shows the estimated Dst and the corrected hourly magnetic disturbances (D_i (t)/cos λ) at the four reference stations computed using the above procedures. The estimated Dst shows that the SSC (≈80 nT) peaked immediately at 8:00 GMT and that a steep negative excursion occurred at approximately 14:00 GMT on March 28, where the maximal intensity of this storm was recorded as ≈−512 nT with caveats of usage of equivalent stations. The main phase of the storm ended at 15:00 GMT, and the recovery phase lasted until 0:00 GMT on March 30. The data from Kakioka were off-scale during 12:00–15:00 GMT on March 28, which coincides with the main phase and is situated immediately after the great jump of 248 nT during 11:00–12:00 GMT. The time series of these reference stations indicates few asymmetric disturbances.

Here, we must stress that the estimated hourly Dst is probably conservative for the following two reasons. The first reason is the lack of proper observations in the dusk–mid-night sector, where the contribution from the storm-time ring current is significant. Here, we used Watheroo instead of Kakioka because the latter was off-scale during the main phase of the storm. Whereas Watheroo recorded the hourly value without a break, Kakioka was also off-scale during 14:06–14:23 GMT (see Parkinson 1946) and may have recorded its hourly value conservatively. Indeed, this magnetic storm peaked in the late evening in Watheroo, and, as expected, the ring current was

[4] http://wdc.kugi.kyoto-u.ac.jp/caplot/index.html.
[5] http://www.geomag.bgs.ac.uk/data_service/data/annual_means.shtml.

Table 1. Magnetic observatories in March 1946 shown in this paper, with their geographic latitude (lat.) and longitude (long.), magnetic latitude (mlat.) and longitude (mlon.), maximal amplitudes of SSC and H of the storm, and their references; their magnetic coordinates were computed using IGRF-12 (Thébault et al. 2015).

Observatory	lat.	long.	mlat.	mlon.	SSC	spot H-range	References
Heramnus[a]	S34°25′	E019°13′	−33.2	80.1	–	523	Ogg (1946)
Honolulu[a]	N36°14′	W158°00′	35.5	−97.8			WDC Kyoto
San Juan[a]	N18°07′	W066°15′	29.6	2.6			WDC Kyoto
Watheroo[a]	S30°19′	E115°52′	−41.8	−174.8	84	>607	Parkinson (1946)
Kakioka	N36°14′	E140°11′	26	−154.4	81	>412	KED
Alibag	N18°38′	E072°52′	9.5	143.2	82	1041	Rao (1946)
Huancayo	S12°02′	W076°20′	−0.6	−7.6	118	1033	Ledig (1946)
Elisabethville	S11°39′	E027°28′	−12.6	93.6	–	990	Scott (1946)
Tucson	N32°15′	W110°50′	40.4	−48.3	128	≈695	Westerman (1946)
Abinger	N50°11′	E000°23′	53	83.2		≈1500	Anon. (1946)

The data at Honolulu and San Juan are only with the hourly resolution acquired from the WDC for Geomagnetism at Kyoto and hence not used for the SSC amplitude and the spot H-range (WDC Kyoto). The Kakioka data are derived from the Kakioka Event Database. The H ranges in Tucson and Abinger are given only with approximation and hence shown with the sign of '≈' for clarification. [a]The reference stations.

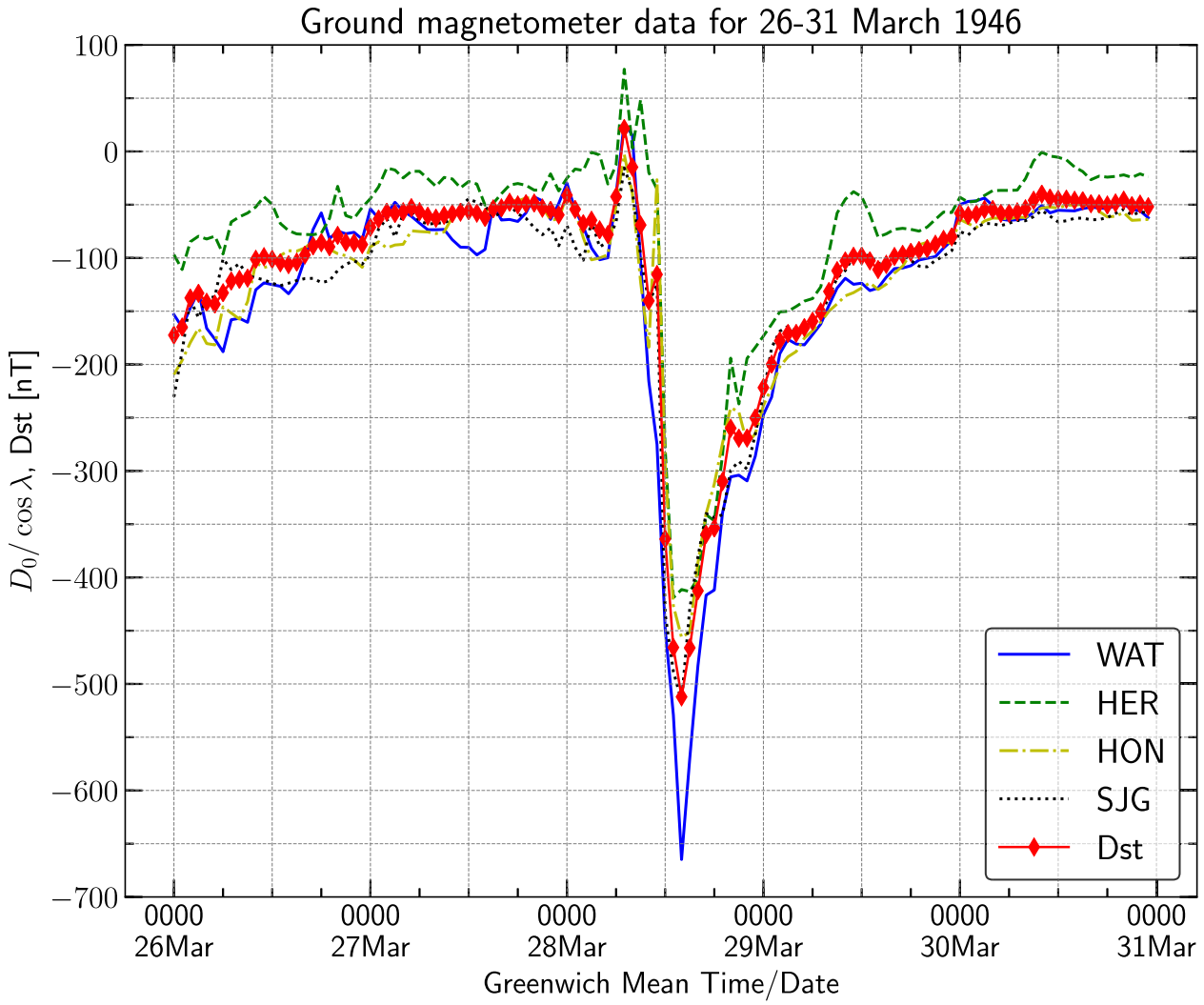

Figure 5. Time series of the estimated Dst and the corrected magnetic disturbances (D_i (t)/cos λ) at the four reference stations: Watheroo (WAT), Hermanus (HER), Honolulu (HON), and San Juan (SJG). These time series span from 0:00 GMT on 1946 March 26 to 23:00 on March 30.

enhanced. Therefore, it will be more realistic to describe its storm intensity as the most negative Dst∗ ≤ −512 nT.

Moreover, its storm intensity may be underestimated because of the time resolution if we employ the 1-h value of Dst. The maximum amplitudes of H/cos λ at Watheroo and Hermanus are >809 and 625 nT, respectively, whereas their hourly values are 665 and 413 nT, respectively. This means the estimated Dst should be much larger at a higher time resolution, as is frequently the case with

large magnetic storms such as the 1859 September storms. In 1859 September, the Colaba spot value of −1760 nT, which was measured at 15-min intervals (Tsurutani et al. 2003), was averaged hourly to −900 nT (+50, −150; Siscoe, Crooker & Clauer 2006; Gonzalez et al. 2011; Cliver & Dietrich 2013).

This magnetic storm is notable in terms of its intensity in comparison with the magnetic storms in the official Dst index issued by WDC Kyoto for the last 63 yr (1957 onward). The intensity (most negative Dst∗ ≤ −512 nT) is situated between the largest magnetic storm in 1989 March (most negative Dst = −589 nT) and the second largest storm in 1959 July (most negative Dst = −429 nT) (World Data Center for Geomagnetism, Kyoto et al. 2015). Extending our survey back in time, this storm is involved in one of the six known superstorms (most negative Dst or Dst∗ ≤ −500 nT; see Hayakawa et al. 2019a, b). Its intensity is quite comparable to a storm in 1903 October/November (most negative Dst∗ ≈ −531 nT; Hayakawa et al. 2020), slightly more moderate than those in 1909 September (most negative Dst∗ ≈ −595 nT; Hayakawa et al. 2019a; Love et al. 2019a) and 1989 March (most negative Dst = −589 nT; Allen et al. 1989; Boteler 2019), and much more moderate than the superstorms in 1921 May (most negative Dst∗ ≈ −907 ± 132 nT; Love et al. 2019b) and 1959 September and 1872 February (Tsurutani et al. 2003; Cliver & Dietrich 2013; Hayakawa et al., 2018, 2019b).

5 AURORAL OVAL AND SPACE WEATHER HAZARDS DURING THE 1946 MARCH STORM

Around the climax of this magnetic storm (12:00–19:00 GMT; Dst∗ < −300 nT), aurorae with a great extension were reported from Watheroo. The aurora started to be visible at 11:35 GMT and lasted at least until 14:15 GMT. This time period almost matches the main-phase duration of the storm. At its climax, a corona aurora was observed, extending beyond the zenith, i.e. 'at 13 h 30 m very bright rays appeared to originate from the arch and converged at a point 10° north of zenith' (Parkinson 1946, p. 298). Because the magnetic latitude of Watheroo is computed as −41°.8, the appearance of the corona aurora yields a magnetic footprint of the equatorward boundary of the auroral oval estimated at ≤41°.8 for an assumed auroral height of ≈400 km (Roach et al. 1960; Ebihara et al. 2017) and a dipole magnetic field. Its absolute value is equivalent to the invariant latitude (O'Brien et al. 1962; fig. 2 of Hayakawa et al. 2019a). This extent is comparable to that of the 1901 October/November storm, in which the auroral oval extended down to 44°.1 in invariant latitude (Hayakawa et al. 2020).

Although the main phase of the storm finished before sunset in the European sector, aurorae had been reported from some European cities such as Abinger and Göttingen. In Göttingen, in particular, 'strong aurora, extending over the zenith' was reported by J. Bartels 'from sunset to about 20^{h} GMT' (Anon 1946, pp. 283–284). This record implies that the auroral oval still extended beyond the zenith of Göttingen (52°.4 MLAT) during the storm recovery phase. These auroral reports were accompanied by space weather hazards such as a dislocation of long-distance radio channels and submarine-cabled telegraphy at Abinger (Anon 1946, p. 283), as well as transformer problems at Port Arthur and Crow River in Canada (Boteler, Pirjola & Nevanlinna 1998).

6 GREAT MAGNETIC DISTURBANCE IN LOW MAGNETIC LATITUDE

As shown in Table 1, the maximal amplitudes of the H-component are close to, or larger than, ≈1000 nT at Alibag, Huancayo, Elisabethville, and Abinger near the storm maximum. These four stations are also indicated by the red circles in Fig. 6. Huancayo, Elisabethville, and Abinger are located on the dayside, whereas Alibag is located on the duskside. Excluding these stations, the amplitudes remained within the range of 500–700 nT (Hermanus and Tucson). Data from Kakioka and Watheroo are off-scale.

Let us first consider the contribution from the storm-time ring current. The ring current is essentially a diamagnetic current surrounding the Earth. The eastward current flows in the inner region, whereas the westward current flows in the outer region (Le, Russell & Takahashi 2004). The intensities of the westward current density (A/m^2) are comparable to those of the eastward current density (Lui, McEntire & Krimigis 1987). However, the volume of the region where the westward current flows is much larger than that where the eastward current flows. Given the dominance of the net westward current (A), the geomagnetic field decreases when the storm-time ring current develops (Ebihara & Ejiri 2000). Observations have shown that the contribution from the storm-time ring current is significant on the duskside (mid-night–dusk-noon; Cummings 1966; Clauer and McPherron 1980; Rastogi, Winch & James 2014). Traditionally, this can be understood as the penetration of hot ions originating from the nightside plasma sheet (Smith & Hoffman 1973; Kozyra et al. 1998; Ebihara et al. 2002). Based on the above accumulated knowledge, we can draw the first inference that *the ring current developed mostly in the mid-night–dusk sector*. The maximum amplitude at Watheroo is described as '>607 nT'. The ambiguity arises from the fact that the data were off-scale. We carefully consider the actual amplitude at Watheroo to be not much larger than the reported value of 607 nT because the off-scale duration lasted only for 17 min (Parkinson 1946). The corrected amplitude, H/cosλ, at Watheroo could have reached a value of ≥809 nT because of the off-scale duration. The maximum amplitude at Alibag is 1041 nT (Rao 1946), which is located approximately 3 h west of Watheroo. The corrected amplitude, H/cos l, was 1055 nT. As the second inference, *the downward field-aligned current associated with the storm-time ring current increased the amplitude at Alibag*. This inference is based on a statistical study by Ohtani et al. (2007). This is consistent with the maximum amplitude at Elisabethville of 990 nT.

Huancayo (−0°.6 MLAT) recorded an amplitude exceeding 1000 nT during the period from 11:00 to 21:30 UT on March 28 (Ledig 1946). Note that the corrected amplitude at San Juan (29°.6 MLAT), which shares almost the same magnetic local time, is ≈500 nT (Fig. 5). Both stations were located in the dawn-noon sector. This large difference between Huancayo and San Juan suggests that a localized current system could have been significant in the dawn-noon sector, and that the contribution from the storm-time ring current could have been smaller than on the duskside. As the third inference, *a strong westward electrojet flowed near the dip equator on the dayside*. Such large amplitudes of the storm-time geomagnetic disturbances have been observed near the dayside dip equator (Rastogi 2006). One such candidate for the westward current is associated with the disturbance dynamo (Blanc & Richmond 1980). Another candidate is the westward current associated with an overshielding (Kelley et al. 1979), which is thought to occur when the IMF turns northward (Kelley et al. 1979; Ebihara et al. 2008; Kikuchi et al. 2010), or when substorms occur (Wei et al. 2009; Ebihara et al. 2014; Hashimoto et al. 2017). Overshielding is also associated with the equatorward extension of the reversed convection centred at mid- or high latitudes (Kelley et al. 1979; Ebihara et al. 2008, 2014; Kikuchi et al. 2010). If this was the case, the earthward penetration of magnetospheric hot ions from the nightside plasma sheet would be impeded by the reversed convection electric field

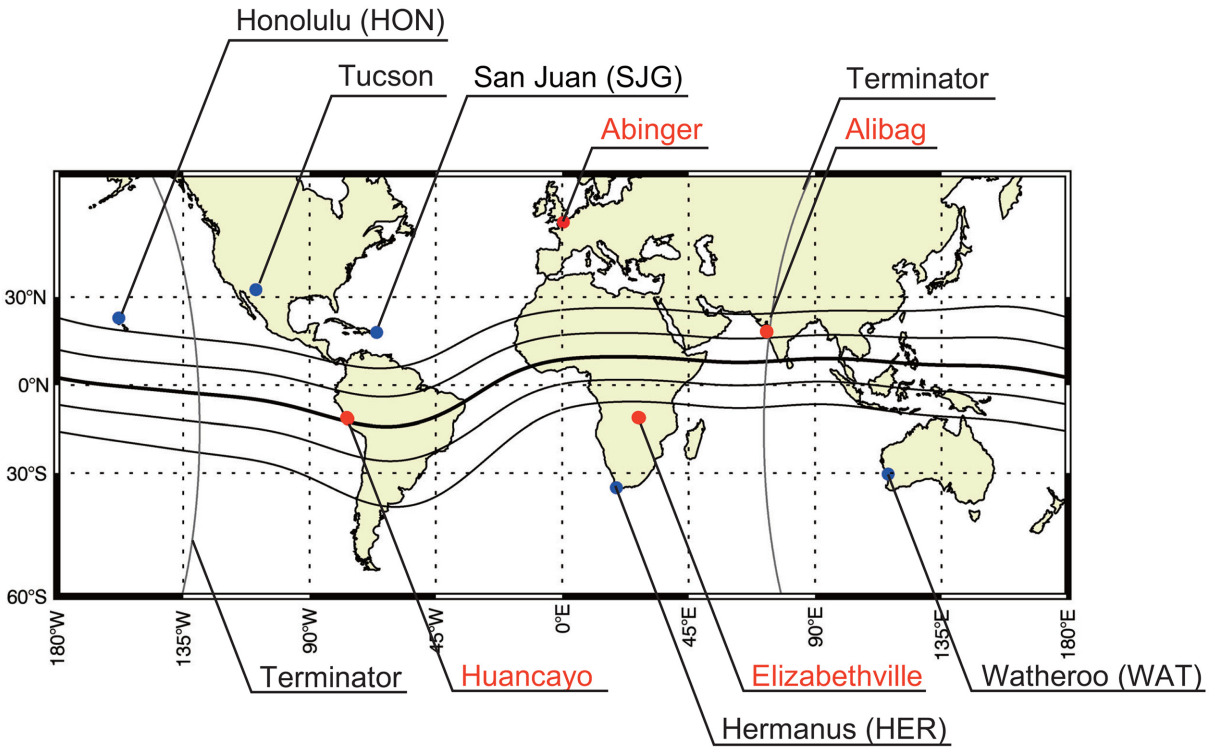

Figure 6. The locations of the observatories and the dip latitudes (0°, ±10°, ±20°) were calculated based on the magnetic inclination at 100-km altitudes with the IGRF-12 model (Thébault et al. 2015). The locations at which the magnetic disturbance is ≥900 nT are shown by the red circles. The terminator at an altitude of 100 km is indicated by the grayish lines.

associated with the overshielding. This results in a reduction of the storm-time ring current and contributes to its decay. For both of these cases, the westward current can be intensified significantly near the magnetic equator owing to the Cowling effect (Chapman 1956). Unfortunately, the time-series data of the magnetic field at Huancayo are unavailable, meaning that we can no longer discuss the cause of the large-amplitude magnetic disturbance there.

7 CONCLUSION

In this article, we analysed an extreme solar-terrestrial storm that occurred in 1946 late March based on contemporary observational records of solar flares, ICMEs, magnetic storms, and the equatorial extension of the auroral oval. This storm occurred in the ascending phase of Solar Cycle 18. At that time, two moderate sunspot groups at approximately the centre of the solar disc caused a major solar flare on March 27. This flare was observed at Kodaikanal and Tashkent at 4:10–4:45 (max. intensity at 4:18) and 4:30–7:32 GMT, respectively. Its intensity was reported to be 3 in the Hα flare area at both observatories, which indicates an area of 600–1200 msh. Close inspections of the Tashkent logbooks reveal that the flare ribbons spanned between these two sunspot groups and the depicted area was even larger (2600–2900 msh) than the reported values. The observational onset at Tashkent occurred after the maximum of the flare, and the maximum flare area was possibly even larger. A statistical comparison shows that this was at least an M-class and most probably an X-class flare.

Following the occurrence of this major flare, an extremely fast ICME was launched. Its arrival is confirmed with a large SSC at 06:35–06:36 GMT on March 28. The SSC amplitude was globally recorded as ≥80 nT, whereas its amplitudes at the nightside (Tucson and Huancayo) were significantly enhanced, probably due to the field-aligned current. The time lag between the source flare and SSC shows the average speed of this ICME ≈1590 km s^{-1}. In combination with the reported SSC amplitude, the downstream solar wind pressure and its density were estimated to be ≈45.5 nPa and ≈12 cm^{-3} for the estimated ICME speed of 1590 km s^{-1} and assuming upstream solar wind pressure 2 nP. Caveats should be noted for its potential error here, as the absence of satellite observations does not allow us the exact timing of ICME launch, makes error margin difficult to establish, and affects other estimates on this basis.

After its arrival, this ICME caused a magnetic superstorm. Its amplitude was so extreme that Kakioka, one of the standard Dst stations, failed to record its full extent. To scale its Dst∗ estimate, we compared the time series of the H-component at three Dst stations (Hermanus, San Juan, and Honolulu) and one equivalent station (Watheroo) after removing their diurnal variations, based upon which we obtained the most negative Dst∗ estimate as ≤−512 nT. This is a conservative estimate because even the Watheroo magnetogram was off-scale during 14:06–14:23 GMT, near its peak, whereas its hourly value was still recorded without a break. Given its location on the duskside, the ring current was most likely enhanced around this magnetic longitude, and hence the most negative Dst∗ estimate may have been even more extreme.

This storm was accompanied by a mid-latitude aurora as well. In particular, a visual report of a corona aurora at Watheroo (−41.8 MLAT) requires the footprint of the magnetic field lines of the

equatorward boundary of the auroral oval as $\leq$41.°8 ILAT, on the basis of the assumption of auroral elevation of $\approx$400 km (Roach et al. 1960). This is comparable with those of magnetic superstorms such as those occurring in 1903 October/November and 1989 March.

Interestingly, during this magnetic superstorm, the amplitude of the magnetic disturbances depends on the MLT and magnetic latitude: (i) The maximum amplitude at Watheroo (mid-night-dusk sector) is '>607 nT'. (ii) The maximum amplitude at Alibag (dusk) is 1041 nT. (iii) The magnetic disturbance recorded at Huancayo (near the dip equator on the day side) is even larger (ΔH $\approx$ 1000 nT) than those at mid-magnetic latitudes (ΔH $\approx$ 600 $\pm$ 100 nT). To explain these disturbances, we drew the following inferences. The storm-time ring current induced the magnetic disturbances mostly in the mid-night-dusk sector. The downward field-aligned current associated with the ring current further intensified the magnetic disturbances at near dusk. A westward electrojet also intensified the magnetic disturbances near the dip equator on the dayside.

Our study reconstructs a case study for a low-frequency, high-intensity solar-terrestrial storm and adds one more case report to known superstorms. Such additions will be beneficial for understanding not only the statistics and variability of such storms (Dst/Dst$*$ $\leq$ $-$500 nT), but also the response of low-latitude magnetograms during magnetic superstorms. Whereas the intensity of the Carrington event in 1859 September was estimated based on the high-time-resolution Colaba magnetogram on the dayside (e.g. Tsurutani et al. 2003; Siscoe et al. 2006; Cliver & Dietrich 2013), our report shows that the high-time-resolution data at low magnetic latitudes can occasionally be enhanced owing to their time resolution and the contributions from the strong westward equatorial electrojet and field-aligned current. In this sense, we need to be cautious when using low-latitude magnetograms to evaluate the intensity of magnetic superstorms and their ring-current intensity.

ACKNOWLEDGEMENTS

This study was financially supported by the Unit of Synergetic Studies for Space of Kyoto University, BroadBand Tower, JSPS Overseas Challenge Program for Young Researchers, the 2020 YLC collaborating research fund, and the research grants for Mission Research on Sustainable Humanosphere from Research Institute for Sustainable Humanosphere (RISH) of Kyoto University, Young Leader Cultivation (YLC) program of Nagoya University, and Grant No. 19–02-00088 by RFBR. We thank Ulugh Beg Astronomical Institute (UBAI) of the Uzbekistan Academy of Sciences for providing the Hα observational logbooks, WDC for Kyoto at Geomagnetism for providing the Dst index and magnetic measurements at Hermanus, San Juan, Honolulu, and Watheroo, Kakioka Event Database for providing data on the SSC and magnetic storms observed in the said observatory, WDC SILSO for providing international sunspot numbers, Solar Science Observatory of the NAOJ for providing copies of the *Quarterly Bulletin on Solar Activity*, and the Paris Meudon Observatory for providing heliograms via the BASS2000 Solar Survey Archive. The Hα Flare reports were prepared using data provided by the USAF Solar Observing Optical Network (SOON) and made available through the NOAA National Centers for Environmental Information (NCEI). AAP is a member of the international team of Modeling Space Weather and Total Solar Irradiance over the Past Century supported by the International Space Science Institute (ISSI), Bern, Switzerland, and ISSI-Beijing, PRC.

REFERENCES

Afanasyeva V.I., 1954, Guide to the Variable Magnetic Field of the USSR. Research Institute of Terrestrial Magnetism, Hydrometeorological Publishing House, Leningrad
Allen J., Frank L., Sauer H., Reiff P., 1989, EOS Trans. Am. Geophys. Union, 70, 1479
Anon, 1946, Terr. Magn. Atmos. Electr., 51, 283
Araki T., 2014, Earth Planets Space, 66, 164
Baker D. et al., 2008, Severe Space Weather Events – Understanding Societal and Economic Impacts. National Academies Press, Washington, DC
Balasubramaniam K. S., Pevtsov A. A., Cliver E. W., Martin S. F., Panasenco O., 2011, ApJ, 743, 202
Blanc M., Richmond A. D., 1980, J. Geophys. Res., 85, A4
Boteler D. H., 2019, Space Weather, 17, 1427
Boteler D. H., Pirjola R. J., Nevanlinna H., 1998, Adv. Space Res., 22, 17
Brueckner G. E. et al. 1995, Sol. Phys., 162, 357
Chapman S., 1956, Nature, 179, 7
Chapman S. C., Horne R. B., Watkins N. W., 2020, Geophys. Res. Lett., 47, e86524
Clauer C. R., McPherron R. L., 1980, J. Geophys. Res., 85, 6747
Clette F., Lefèvre L., 2016, Sol. Phys., 291, 2629
Cliver E., Dietrich W., 2013, J. Space Weather Space Clim., 3, A31
Cummings W. D., 1966, J. Geophys. Res., 71, 4495
Daglis I. A., Thorne R. M., Baumjohann W., Orsini S., 1999, Rev. Geophys., 37, 407
D'Azambuja L., 1947, Quarterly Bulletin on Solar Activity, Nos. 69–76. Swiss Federal Observatory, Eidgenössische Sternwarte Zürich
Domingo V., Fleck B., Poland A. I., 1995, Sol. Phys., 162, 1
Ebihara Y., Ejiri M., 2000, J. Geophys. Res., 105, 15843
Ebihara Y., Ejiri M., Nilsson H., Sandahl I., Milillo A., Grande M., Fennell J. F., Roeder J. L., 2002, Geophys. Res. Lett., 29, 20
Ebihara Y., Nishitani N., Kikuchi T., Ogawa T., Hosokawa K., Fok M.-C., 2008, J. Geophys. Res. Space Phys., 113, A01213
Ebihara Y., Tanaka T., Kikuchi T., 2014, J. Geophys. Res. Space Phys., 119, 7281
Ebihara Y., Hayakawa H., Iwahashi K., Tamazawa H., Kawamura A. D., Isobe H., 2017, Space Weather, 15, 1373
Ferraro V. C. A., Unthank H. W., 1951, J. Atmos. Terr. Phys., 16, 136
Gonzalez W. D., Joselyn J. A., Kamide Y., Kroehl H. W., Rostoker G., Tsurutani B. T., Vasyliunas V. M., 1994, J. Geophys. Res., 99, 5771
Gonzalez W. D., Echer E., Tsurutani B. T., Clúa de Gonzalez A. L., Dal Lago A., 2011, Space Sci. Rev., 158, 69
Gopalswamy N, 2018, Extreme Events in Geospace. Elsevier, Amsterdam
Hale G. E., 1929, ApJ, 70, 265
Hashimoto K. K., Kikuchi T., Tomizawa I., Nagatsuma T., 2017, J. Geophys. Res. Space Phys., 122, 10851
Hayakawa H. et al. 2018, ApJ, 862, 15
Hayakawa H. et al. 2019a, MNRAS, 484, 4083
Hayakawa H. et al. 2019b, Space Weather, 17, 1553
Hayakawa H. et al. 2020, ApJL, 897, L10
Hinterreiter J., Veronig A. M., Thalmann J. K., Tschernitz J., Pötzi W., 2018, Sol. Phys., 293, 38
Jones H. S., 1955, Sunspot and Geomagnetic-Storm Data Derived from Greenwich Observations, 1874–1954. Her Majesty's Stationery Office, London
Karinen A., Mursula K., 2005, Ann. Geophys., 23, 475
Kelley M. C., Fejer B. G., Gonzales C. A., 1979, Geophys. Res. Lett., 6, 301
Kikuchi T., Ebihara Y., Hashimoto K. K., Kataoka R., Hori T., Watari S., Nishitani N., 2010, J. Geophys. Res., 115, A05209
Kozyra J. U., Jordanova V. K., Borovsky J. E., Thomsen M. F., Knipp D. J., Evans D. S., McComas D. J., Cayton T. E., 1998, J. Geophys. Res., 103, 26285
Lakhina G. S., Tsurutani B. T., 2018, Extreme Events in Geospace. Elesevier, Amsterdam
Le G., Russell C. T., Takahashi K., 2004, Ann. Geophys., 22, 1267
Ledig P. G., 1946, Terr. Magn. Atmos. Electr., 51, 293

Lefèvre L., Vennerstrøm S., Dumbović M., Vršnak B., Sudar D., Arlt R., Clette F., Crosby N., 2016, Sol. Phys., 291, 1483
Lockwood M., Owens M. J., Barnard L. A., Bentley S., Scott C. J., Watt C. E., 2016, Space Weather, 14, 406
Lockwood M., Chambodut A., Barnard L. A., Owens M. J., Clarke E., Mendel V., 2018, J. Space Weather Space Clim., 8, A53
Love J. J., Hayakawa H., Cliver E. W., 2019a, Space Weather, 17, 37
Love J. J., Hayakawa H., Cliver E. W., 2019b, Space Weather, 17, 1281
Lui A. T. Y., McEntire R. W., Krimigis S. M., 1987, J. Geophys. Res., 92, 7459
Miyake F., Usoskin I. G., Poulianov S., 2019, Extreme Solar Particle Storms. IOP, London
O'Brien B. J., Laughlin C. D., Van Allen J. A., Frank L. A. 1962, J. Geophys. Res., 67, 1209
Ogg A., 1946, Terr. Magn. Atmos. Electr., 51, 298
Ohtani S., Ebihara Y., Singer H. J., 2007, J. Geophys. Res. Space Phys., 112, A05202
Oughton E. J., Skelton A., Horne R. B., Thomson A. W. P., Gaunt C. T., 2017, Space Weather, 15, 65
Parkinson W. C., 1946, Terr. Magn. Atmos. Electr., 51, 295
Rao M. P., 1946, Terr. Magn. Atmos. Electr., 51, 292
Rastogi R. G., 2006, Earth Planets Space, 58, 645
Rastogi R. G., Winch D. E., James M. E., 2014, Earth Planets Space, 53, 969
Riley P., Baker D., Liu Y. D., Verronen P., Singer H., Güdel M., 2018, Space Sci. Rev., 214, 21
Roach F. E., Moore J. G., Bruner E. C., Jr, Cronin H., Silverman S. M., 1960, J. Geophys. Res., 65, 3575
Scott W. E., 1946, Terr. Magn. Atmos. Electr., 51, 281
Shinbori A., Tsuji Y., Kikuchi T., Araki T., Watari S., 2009, J. Geophys. Res., 114, A04217
Shinbori A. et al. 2012, J. Geophys. Res., 117, A08322
Siscoe G. L., Formisano V., Lazarus A. J., 1968, J. Geophys. Res., 73, 4869
Siscoe G., Crooker N. U., Clauer C. R., 2006, Adv. Space Res., 38, 173
Smith P. H., Hoffman R. A., 1973, J. Geophys. Res., 78, 4731
Sugiura M., 1964, Ann. Int. Geophys. Year, 35, 9
Švestka Z., 1976, Solar Flares. Springer-Verlag, Berlin
Thébault E. et al. 2015, Earth Planets Space, 67, 79
Toriumi S., Schrijver C. J., Harra L. K., Hudson H., Nagashima K., 2017, AJ, 834, 56
Tsurutani B. T., Gonzalez W. D., Lakhina G. S., Alex S., 2003, J. Geophys. Res., 108, 1268
World Data Center for Geomagnetism, Kyoto, Nose M., Iyemori T., Sugiura M., Kamei T., 2015, Geomagnetic Dst Index
Wei Y. et al. 2009, J. Geophys. Res., 114, A12209
Westerman C. E., 1946, Terr. Magn. Atmos. Electr., 51, 290
Youssef M., 2012, NRIAG J. Astron. Geophys., 1, 172

APPENDIX: TASHKENT ARCHIVAL MATERIALS

Catalogue of solar rapid processes of Tashkent Astronomical Observatory for the period 03.04.1945–29.12.1949–DOI: 10.7910/DVN/9GQBSL
Journal of spectrohelioscopic observations № 42, DOI: 10.7910/DVN/YLYMYV
Slonim, Yu. M., 1953. *Solar Activity in the year 1946*, Trudy Tashkentskoj Astronomicheskoj Observatorii, DOI: 10.7910/DVN/IFW1FU

This paper has been typeset from a TEX/LATEX file prepared by the author.